Electronic Supplementary Material (ESI) for **New Journal Chemistry**.

Supplementary data

Enhanced PMS/O_2 Activation by Self-Crosslinked Amine Gluteraldehyde/Chitosan-Cu Biocomposite for Efficient Degradation of HEPES as Biological Pollutant and Selective Allylic Oxidation of Cyclohexene

Sara Movahedian[a], Alireza Faraji*[,a,b] and Fatemeh Ashouri[c]

[a]*Department of Organic Chemistry, Faculty of Pharmaceutical Chemistry, Tehran Medical Sciences, Islamic Azad University, Tehran, Iran.*

[b]*Nutrition and Food Sciences Research Center, Tehran Medical Sciences, Islamic Azad University, Tehran, Iran.*

[c]*Department of Applied Chemistry, Faculty of Pharmaceutical Chemistry, Tehran Medical Sciences, Islamic Azad University, Tehran, Iran.*

Corresponding author. Tel.: +98 21 22640051; fax: +98 21 22600099.
E-mail address: alireza_ch57@yahoo.com, a.faraji@iaups.ac.ir

Text. 1S. *Experimental reagent and materials*

Iron (II)-chloride tetrahydrate ($FeCl_2 \cdot 4H_2O$), Iron (III)-chloride hexahydrate ($FeCl_3 \cdot 6H_2O$), hydrochloric acid (HCl, 37%), sodium hydroxide solution (NaOH, 1.5 M), ethanol (EtOH), ammonia solution (NH_3, 25%), tetraethyl orthosilicate (TEOS, $Si(OC_2H_5)_4$), *N*-(2-Aminoethyl)-3-aminopropyltrimethoxysilan (APTS, $H_2N(CH_2)_2NH(CH_2)_3Si(OCH_3)_3$), acetic acid ($CH_3CO_2H$), chitosan ,glutaraldehyde solution ($OHC(CH_2)_3CHO$, 25%) and $CuCl_2.2H_2O$ were obtained from Merck, Fluka and Sigma-Aldrich Co., Ltd., and utilized without futher purification for MS/(AgC)-Cu NP preparation. Potassium peroxymonosulfate (Oxone, PMS, $KHSO_5.0.5KHSO_4 \cdot 0.5K_2SO_4$), methylene blue (MB), methylene orange (MO), bisphenol A (BPA), *N,N*-dihydroxypyromellitimide (NDHPI, $C_{10}H_6N_2O_6$) and Cyclohexene (C_6H_{10}) were purchased from Sigma-Aldrich and utilized for dye degradation and aerobic oxidation processes without further purification.

Text. 2S. *Characterization of biocomposite*

the instrument for characterization and analyze of products are mentioned blow: ICP-AES (Perkin-Elmer ICP/6500); AAS (Analytik Jena-nov AA300); ICP-OES (SPECTRO ARCOS, Germany); Brunauer–Emmett–Teller (BET; BELSORP MINI II, BEL, Japan); TEM (Philips 501 microscope,80 kV voltage); SEM (Tecnai F30TEM operating at 300 Kv); FT-IR (Shimadzu Varian 4300 Fourier Transform Infrared spectrometer, KBr pellets); UV-DRS (UV- 160 A, Shimadzu, Japan) TGA (Perkin-Elmer TG-DTA 6300, heating rate of 15 °C/min); XPS (PerkinElmer PHI 5000CESCA system, B.P= 9-10 Torr; XRD (Bruker D8 Advance diffractometer, CuKa radiation, 40 Kv, 20 mA) & VSM (BHV-55 VSM). LC-MS (HP 6890/5973 GC/MS, Shimadzu GC-16A gas chromatograph (GL-16, 5 m -3 mm OV-17 column, 60–220 °C (10 °C/min), Inj. 230 °C, Det. 240 °C).

Text 3S. Analytical methods

The dosage of HEPES was determined using High-Performance Liquid Chromatography (HPLC) system equipped with an Amaze TH column (100 mm×3.0 mm, 3um, 100 A). A binary mixture of acetonitrile/ water/ammonium format at a certain ratio was applied as mobile phase. The flow rate of eluent was set at 0.6 mL/min, while the injection volume was set at 3.0 mL, thermostatted at 30 ºC. Furthermore, Methyl orange (MO), Methylene Blue (MB), and Bisphenol A (BPA) were measured at 466 nm, 660 nm, and 265 nm, respectively, by a spectrometer (UV-1800 PC, Shanghai Mapada Spectrum Instrument Co.,LTD). The leached concentrations of Cu ions were quantified by inductively coupled plasma atomic emission spectroscopy (ICP-AES, Perkin Elmer, Optima 8000, USA). The total organic carbon was measured by a TOC analyzer (Muti N/C 2000, Germany).

PMS decomposition measurement: The PMS concentrations were measured with a modified colorimetric method using potassium iodide by spectrophotometer. At selected time intervals, 0.1 mL of TC solution was periodically withdrawn with a syringe and dispersed into a prepared 4.9 mL KI:$NaHCO_3$ stock solution (4.15:1 w/w in 100 mL ultrapure water). After reaction for 5 min, the concentration of PMS was examined by observing the absorbance maxima peaks of PMS at 352 nm.

Reusability test: The spent MS-(A*g*C)/Cu was separated with an external magnet and washed with water/EtOH under ultrasonic conditions, and then reutilized in the next consecutive cycles.

Table 1S. Chemical structures and capabilities of the selected pollutants.

Sample	λ_{max} (nm)	Mw (g/mol)	Name (IUPAC)	Molecular structure
Methylene orange **(MO)**	466	327.33	Sodium 4-{[4-(dimethylamino)phenyl]diazenyl}benzene-1-sulfonate	
Methylene blue **(MB)**	664	319.85	[7-(Dimethyl- amino)phenothiazin-3-ylidene]-dimethyla- zanium chloride	
Bisphenol A **(BPA)**	265	228.29	4-[2-(4-hydroxyphenyl)propan-2-yl]phenol	

Table 2S. Identified HEPES degradation intermediates in the PMS/MS-(A*g*C)/Cu.

[In]	Name	ESI (+) MS (*m/z*)	Structure	Differences from HEPES
P1	1,4-diethylpiperazine	208.09	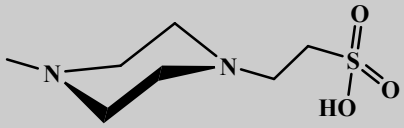	$-CH_2$ -OH
P2	1,4-diethylpiperazine	142.15	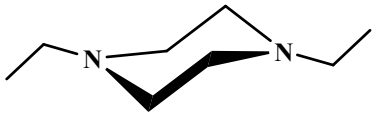	-OH $-SO_3H$
P3	1-ethyl-4-methylpiperazine	128.13	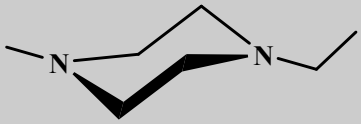	$-CH_2$ -OH $-SO_3H$
P4	Piperazine	86.08	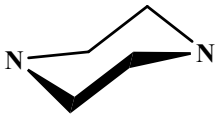	-2 C_2H_4 -OH $-SO_3H$
P5	2-(4-ethylpiperazin-1-yl)ethane-1-sulfonic acid	222.10		-OH
P6	2-(4-methylpiperazin-1-yl)ethane-1-sulfonic acid	208.09	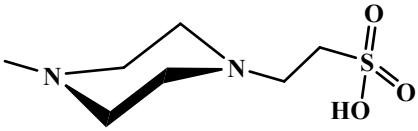	$-CH_2$ -OH
P7	2-(4l2-piperazin-1-yl)ethane-1-sulfonic acid	194.07	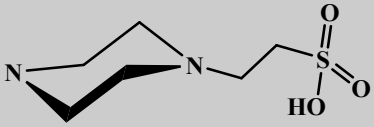	$-C_2H_4$ -OH

Table 3S. Comparison of catalytic activity of MS-(A*g*C)/Cu whit various catalytic systems.

Pol.	Catalytic System	*t* (min)	Oxidant [c]	Efficiency (%)	pH	[Ref]
MB	SBMC [0.4 g/L][1]	3	H_2O_2 [39 mmol/L]	98.5	3.00	[1]
	Magnesium porphyrin [5.0 mg] [2]	25	H_2O_2 [4.0 mL]	82.0	6.00	[2]
	Fe@S-1 [50 mg] [3]	30	H_2O_2 [4.0 mL]	100	2.00	[3]
	MgCoAl-LDH [1.0 mg][4]	40	PMS [1.0 mmol/L]	100	6.00	[4]
	$CuFe_2O_4$@ZIF-67 [100 mg/L][5]	30	PMS [100 mg/L]	98.9	6.40	[5]
	CuCo-ZIF [50 mg/L][6]	100	H_2O_2 [0.1 mol/L]	98.0	3.00	[6]
	Co_3O_4/CoO/$NaHSO_3$ [0.6 g/L]	40	$NaHSO_3$[2.0 g/L]	90.7	6.38	[7]
	Ce-doped UiO-67- 400/H_2O_2 [1.0 g/L][7]	30	H_2O_2 [7 mmol/L]	94.1	3.00	[8]
	$Fe_{41}Co_7Cr_{15}Mo_{14}C_{15}B_6Y_2$ [0.5 g/L]	30	H_2O_2 [4 mmol/L]	98.0	5.00	[9]
	Mg/Co $(OH)_2$ [1.0 g/L]	120	H_2O_2 [10 mg/L]	99.6	>7.0	[10]
	$NbCeO_x$ [20 mg][8]	60	H_2O_2 [200 µL]	83.0	5.10	[11]
	$FeCo_2O_4$-N-C-400 [0.010 g][9]	10	PMS [0.5 g/L]	100	Natural	[12]
	$FeMnO_3$ [0.2 g/L]	60	PMS [2.0 g/L]	98.0	6.70	[13]
	Fe_3O_4@MnO_2 [300 mg/L]	30	PMS [20 mM]	100	7.94	[14]
	CS-Fe [10000 mg/L][10]	40	H_2O_2 [1200 mg/L]	99.0	Natural	[15]
	MS-(A*g*C)/Cu [0.5 g/L]	60	PMS [1.5 mM]	97.3	7.00	**This work**
MO	MOP[11]	20	H_2O_2 [2.0 mL]	98.0	1.70	[16]
	CC-MIL-10-DCD-1000 [0.1 g/L][12]	30	PMS [0.3 mM]	99.0	7.00	[17]
	ACP-800 [0.5 g/L][13]	80	PMS [1.6 mM]	100	3.50	[18]
	FOC [1.0 mg/mL][14]	50	H_2O_2 [2.0 M]	100	3.00	[19]
	Ni/HAP/$CoFe_2O_4$ [0.04 mg][15]	90	H_2O_2 [1.0 mL]	90.0	3.50	[20]
	FeCo-MCM-41[0.2 g]	60	PMS [0.075 mM]	95.65	5.60	[21]
	CuO NLs [7.0 mL,53 µg/ml][16]		H_2O_2 [1.0 mL]	100	-	[22]
	Cu_2O-Cu/C	20	H_2O_2 [0.03 M]	100	3.00	[23]
	MS-(A*g*C)/Cu [0.5 g/L]	50	PMS [1.5 mM]	98.0	7.00	**This work**
BPA	$CuFe_2O_4$-$CoFe_2O_4$ [20 mg/L]	100	PMS [0.3 g/L]	99.3	7.01	[24]
	13%-Mn-FeBC [0.5 g/L][17]	120	PMS [4.0 mM]	100	12.0	[25]
	CuO/Cu_2O [500mg/L][18]	10	PMS [150mg/L]	99	11.0	[26]
	CuO-CN [0.5 g/L][19]	30	PMS [100 mg/L]	80	-	[27]
	MS-(A*g*C)/Cu [0.5 g/L]	30	PMS [1.5 mM]	99.1	7.00	**This work**
HEPES	OBW/HP@CoNP [50 ppm][20]	20	PMS [1.25 mM]	98	7.40	[28]
	MS-(A*g*C)/Cu [0.5 g/L]	30	PMS [1.5 mM]	98.3	7.00	**This work**

[1] Fenton sludge was converted into magnetic sludge-based biochar.
[2] Magnesium (II) porphyrin with the ligand hexamethylenetetramine.
[3] Zeolite encapsulated Fe nanocatalyst.
[4] Layered double hydroxide(LDH).
[5] Zeolitic imidazolate framework-67(ZIF-67).

[6] Zeolitic imidazolate framework(ZIF).
[7] Ce-doped MOF (Metal–organic framework)/calcination temperature of catalyst 400 °C.
[8] Mixed niobium-cerium oxide.
[9] Calcined nitrogen-containing carbon//$FeCo_2O_4$ composites.
[10] Fenton chitosan-Fe catalyst.
[11] Magnetite nanoparticles (Fe_3O_4-NPs)/orange peel.
[12] Dicyandiamide immobilized on the surface of carbon cloth.
[13] Activated carbon using pistachio.
[14] $Fe_3C/Fe_3O_4/C$.
[15] Hydroxyapatite.
[16] Cupric oxide nanoleaves.
[17] x-Mn-FeBC, where × represents the mass percentage of KMnO4 to DS (dry sludge).
[18] A novel B-doped CuO/Cu_2O composite material.
[19] Copper oxide/graphitic carbon nitride.
[20] Ostrich bone waste/Hydrogen peroxide.

Table4S. Comparison of catalytic activity of MS-(A*g*C)/Cu in selective aerobic oxidation of cyclohexene whit various catalytic systems.

No.	Catalytic System	*X* ,%	*S*, %			[Ref]
			CY-*epoxy*	CY-*ol*	CY-*one*	
1	$CoFe_2O_4$, 80 °C, 6h, CH_3CN, O_2	63.0	8.0	9.0	25.0	[29]
2	PVDA1-PMo [1], 130°C, 7h, CH_3CN, O_2	85.7	-	-	51.9	[30]
3	Ti-Beta zeolite, 59.85 °C, 2 h, CH_3CN, H_2O_2	27.9				[31]
4	MoCeNR[2], 80°C, 2 h, Toluene, TBHP	98.9	97.3	0.90	1.80	[32]
5	Cu-g-C_3N_4[3], 75 °C, 6 h, CH_3Cl, O_2	82.0	55.0			[33]
6	Cu-MOF-74, 25°C, 24 h, O_2	35.0	-	25.0	61.0	[34]
7	Co-MOF-74, 25°C, 24h, O_2	31.0	-	35.0	59.0	[34]
8	SBA15. DAFO.Pd(II)[4],60 °C,12 h,CH_3CN, H_2O_2	89.3	-	9.10	16.3	[35]
9	LaCuODA[5], 75 °C, 24h, O_2	67.0	-	40.0	55.0	[36]
10	LaCoODA[6], 75 °C, 24 h, O_2	85.0	-	25.0	75.0	[36]
11	CuO FL2[7], 80°C, 24 h, CH_3CN, O_2	97.6	-	-	64.1	[37]
12	ZnMOF-74, 80°C, 4 h, O_2	66.5	12.5	65.4	13.9	[38]
13	NiMOF-74, 80°C, 4 h, O_2	59.0	8.70	74.3	13.3	[38]
14	CoMOF-74, 80°C, 4 h, O_2	52.3	18.9	29.4	22.2	[38]
15	Co(II)-L@nano-SiO_2, 75°C, 8 h, CH_3CN, O_2	61.0	6.50	10.3	46.9	[39]
16	AgCN[8], 60 °C 20 h, CH_3CN, H_2O_2	~100	76.0	-	-	[40]
17	Ti-PMO-S10 [9],70 °C, 25 h, CH_3CN, TBHP	30.5	93.8	-	3.2	[41]
18	Ru/TiO_2 NFs [10], 75 °C, 4.5 h, O_2	95.0	7.00	11.0	80.0	[42]
19	$LaCoO_3$, 80°C, 6 h, TBHP /O_2	89.8	-	-	47.8	[43]
20	Co_5Ce_5/ γ-Al_2O_3, 80 °C, 6 h, O_2	84.0	-	30.0	38.0	[44]
21	MS-(A*g*C)/Cu, NDHPI, 80 °C, ACN, O_2	91.8	5.40	9.10	85.3	**This work**

[1]Heteropolyacid-based poly ionic liquids.
[2]Nanorods.
[3] Catalysts consisting of Cu single atoms anchored on graphitic carbon nitride.
[4]4, 5-diazofluorene-9-one (DAFO).
[5] $\{[La_2Cu_3(\mu\text{-}H_2O)(ODA)_6(H_2O)_3].3H_2O\}_n$.
[6]$\{[La_2Co_3(ODA)_6(H_2O)_6].12H_2O\}_n$ / m; i: flower (FL).
[7] Flowers (FLs).
[8] Silver cyanide.
[9] Ti-containing Periodic Mesoporous Organosilica (PMO).
[10] Ruthenium- Nanofibers (NFs).

Table 5S. Commercial price used for fabrication of MS-(A*g*C)/Cu.

Material	CAS. Number	V (mL) or W (g)	Price ($.g^{-1})
$FeCl_2 \cdot 4H_2O$	13478-10-9	0.20 g	0.020
$FeCl_3 \cdot 6H_2O$	10025-77-1	0.40 g	0.063
HCl	Dr Mojallali,Co.	3.0 mL	0.003
NaOH	Arvand parak, Co.	6.00 g	0.053
NH_4 OH	Dr Mojallali,Co.	4.0 mL	0.013
EtOH	Simin Tak, Co.	40 mL	0.030
TEOS	78-10-4	0.6 mL	0.050
APTS	13822-56-5	0.1 mL	0.050
Chitosan	9012-76-4	0.10 g	0.017
AcOH	64-19-7	0.4 mL	0.030
Glutaraldehyde	Simin Tak, Co.	2.0 mL	0.040
$Cu(OAc)_2$	6156-78-1	0.25 g	0.017
		Total price ($.g^{-1})	0.386

Table 6S. Screening data for the cost of the various systems for degradation of 1m^3 HEPES.

No.	Pollutant/m^3	Catalytic system	Cost (**$** /m^3)	[Ref]
1	Tetracycline	PS+γ-Fe_2O_3-CeO_2	0.106	[45]
2	Ketoprofen	PS+Fe^{2+}	0.517	[46]
3	Ketoprofen	PS+Thermal	44.41	[46]
4	Ketoprofen	PS+UV	0.176	[46]
5	HEPES	PMS+MS-(A*g*C)/Cu	27.57	This work

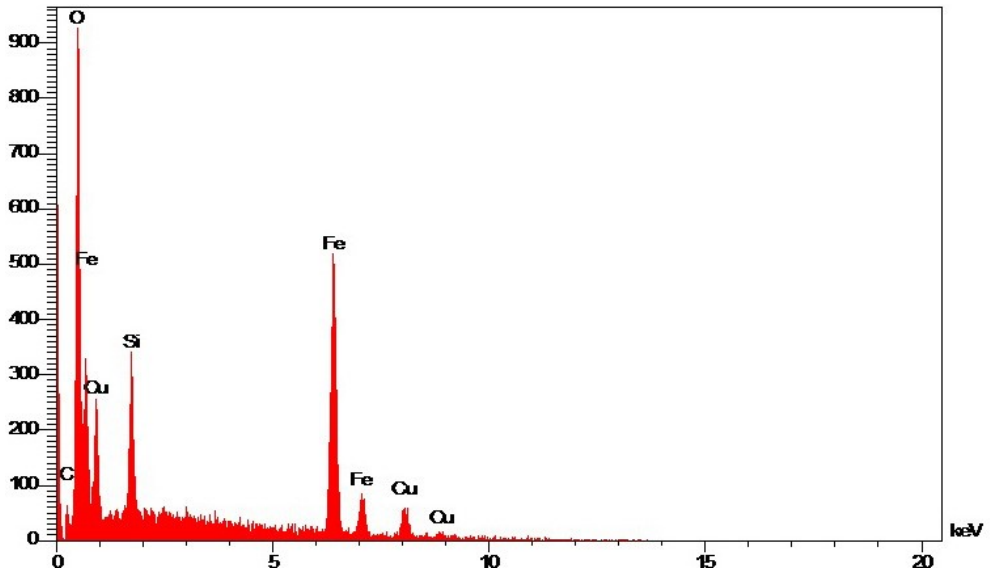

Fig 1S. EDS spectrum of MS-(A*g*C)/Cu.

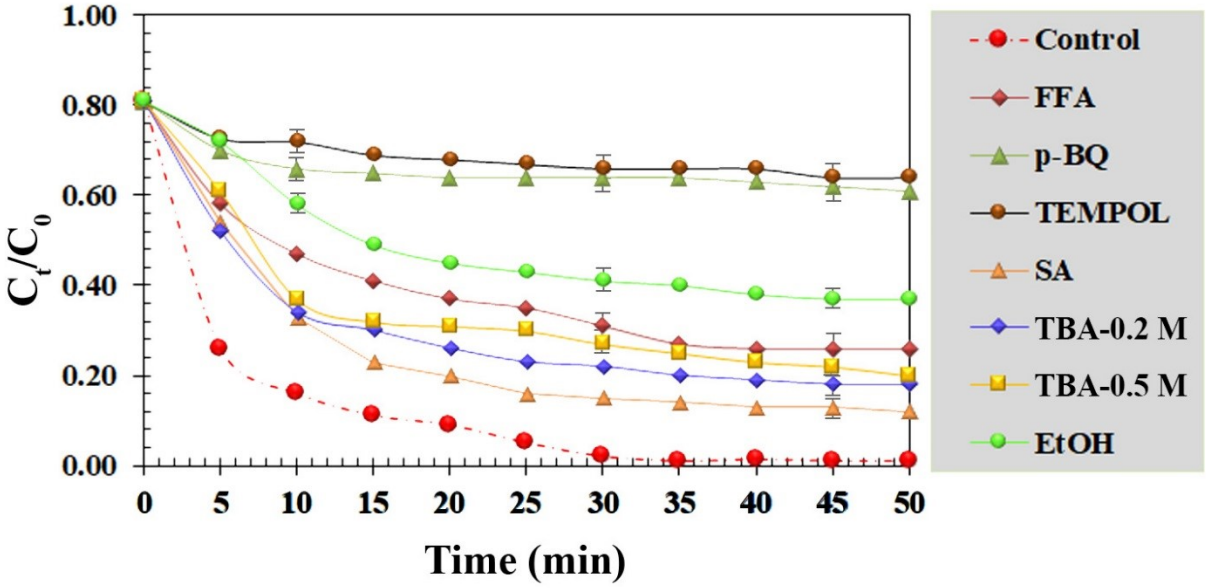

Fig.**2S**. Effect of quenching scavengers on degradation efficiency (%) for HEPES degradation [[MS-(A*g*C)/Cu]$_o$= 0.5 g/L, [HEPES]$_o$= 10 mg/L, pH = 7.0, T= 25 ^{o}C, [PMS]$_o$= 1.5 mM)].

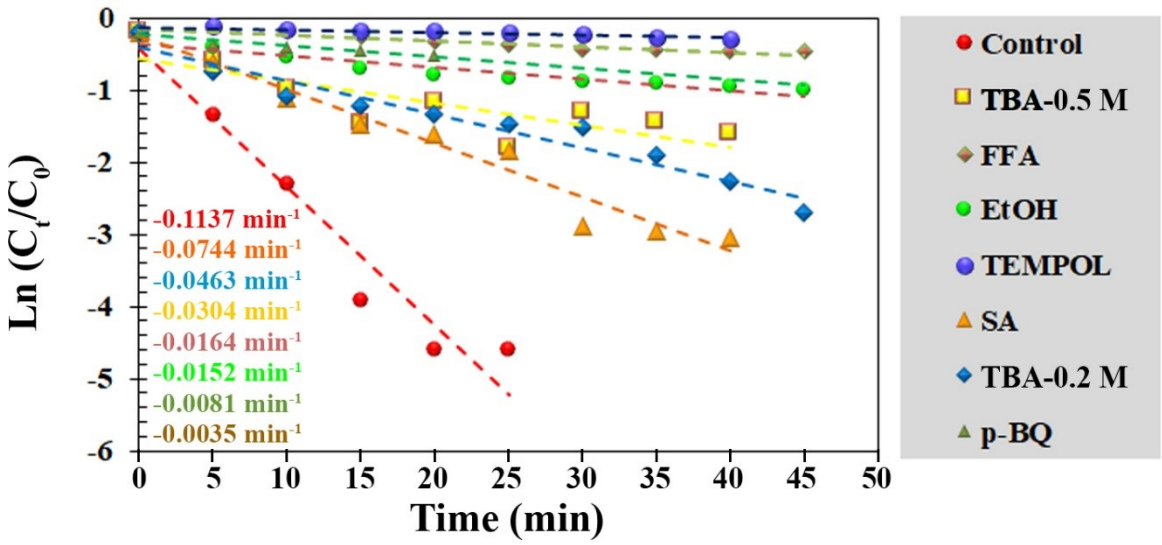

Fig.3S. Effect of quenching scavengers on The reaction rates of HEPES degradation [[MS-(AgC)/Cu]$_o$= 0.5 g/L, [HEPES]$_o$= 10 mg/L, pH = 7.0, T= 25 ^oC, [PMS]$_o$= 1.5 mM)].

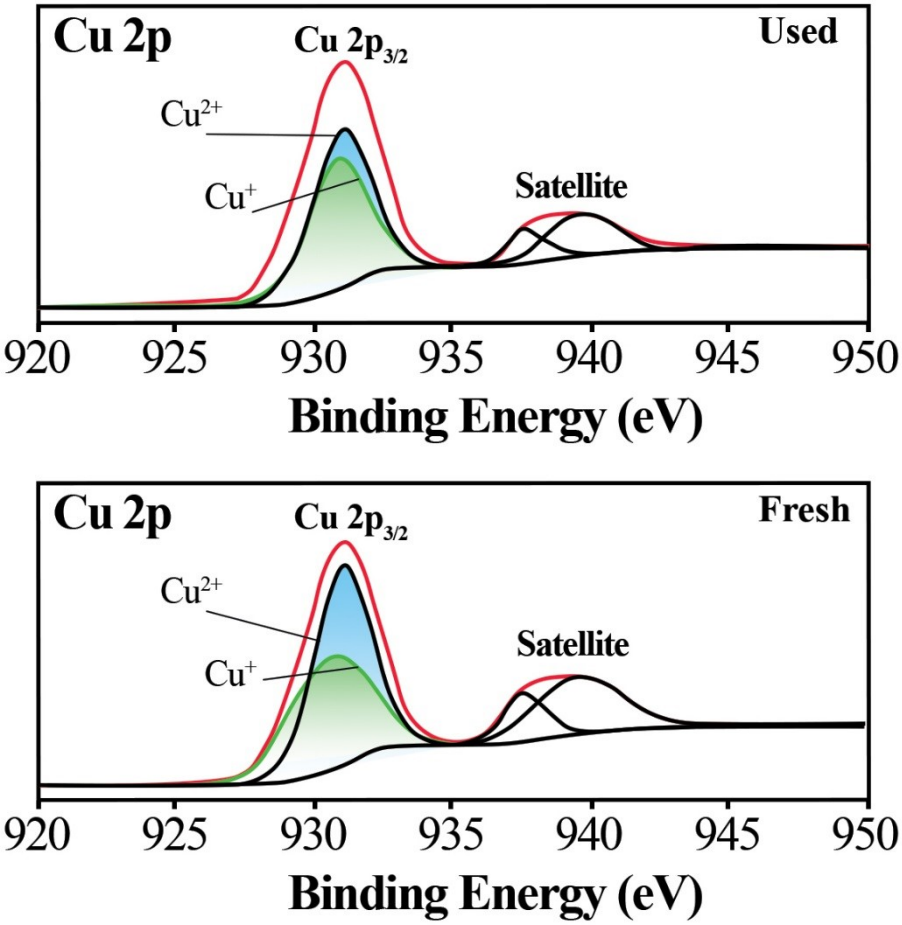

Fig.**4S**. XPS spectrum of Cu2p in (**A**) fresh, and (**B**) used MS-(A*g*C)/Cu.

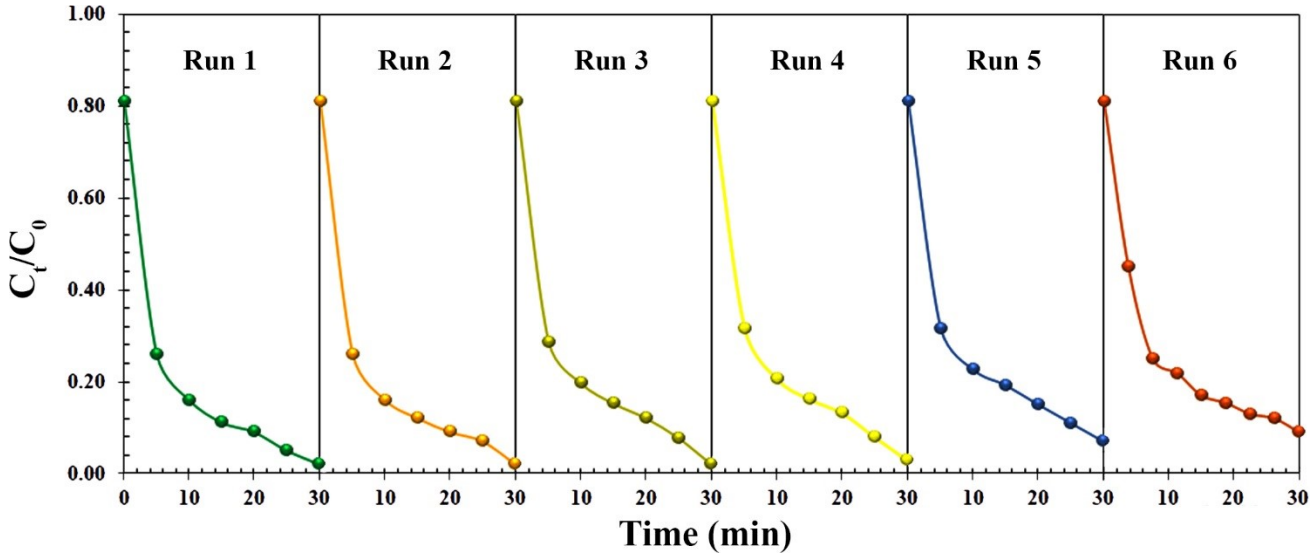

Fig. 5S. Long-term stability of MS-(A*g*C)/Cu in degradation of HEPES [[MS-(A*g*C)/Cu]$_o$= 0.5 g/L, [HEPES]$_o$= 10 mg/L, pH = 7.0, T= 25 ^oC, [PMS]$_o$= 1.5 mM)].

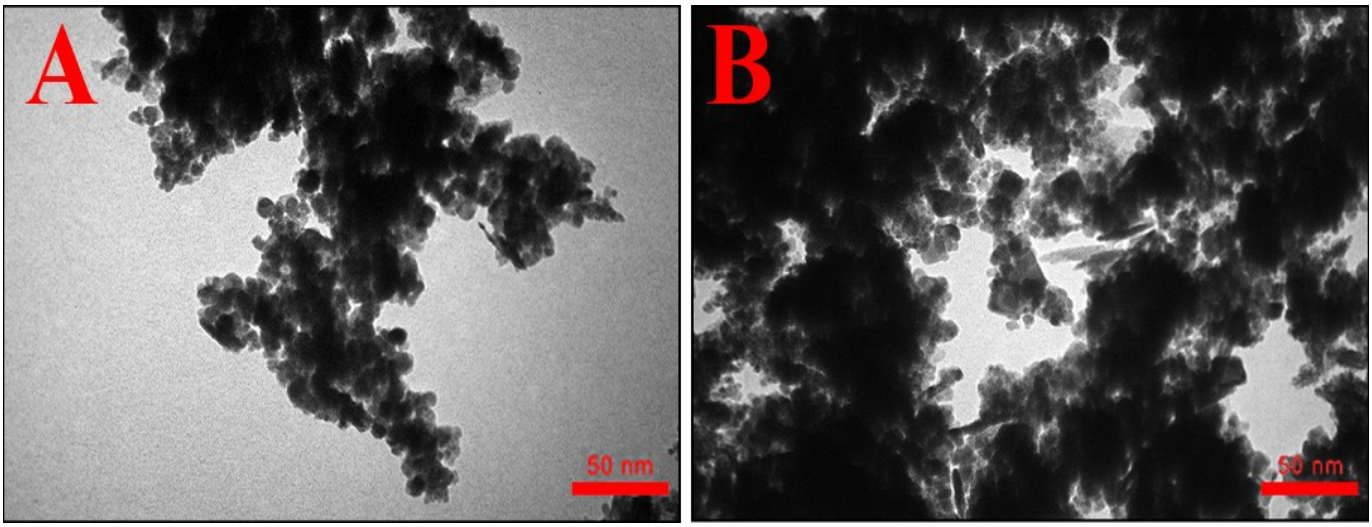

Fig. 6S. Selected TEM images of used MS-(A*g*C)/Cu for (**A**) four times, and (**B**) seven times in HEPES degradation.

References

[1] Ye G, Zhou J, Huang R, Ke Y, Peng Y, Zhou Y, Weng Y, Ling C, Pan W. Magnetic sludge-based biochar derived from Fenton sludge as an efficient heterogeneous Fenton catalyst for degrading Methylene blue. Journal of Environmental Chemical Engineering. 2022 Jan 21:107242.

[2] Ezzayani K, Khelifa AB, Guesmi A, Hamadi NB, Abd El-Fattah W, Nasri H. Application of a new synthesized magnesium porphyrin complex in the degradation of methylene blue dye. Journal of Molecular Structure. 2022 Jun 15;1258:132663.

[3] Guo H, Chen L, Zhang X, Chen H, Shao Y. Silicalite-1 Zeolite Encapsulated Fe Nanocatalyst for Fenton-like Degradation of Methylene Blue. Chinese Journal of Chemical Engineering. 2022 Mar 23.

[4] Wang L, Wang Y, Lv W, Yao Y. Activation of peroxymonosulfate by MgCoAl layered double hydroxide: Potential enhancement effects of catalyst morphology and coexisting anions. Chemosphere. 2022 Jan 1;286:131640.

[5] Wu X, Sun D, Ma H, Ma C, Zhang X, Hao J. Activation of peroxymonosulfate by magnetic CuFe2O4@ ZIF-67 composite catalyst for the study on the degradation of methylene blue. Colloids and Surfaces A: Physicochemical and Engineering Aspects. 2022 Jan 7:128278.

[6] Luong TH, Nguyen TH, Nguyen BV, Nguyen NK, Nguyen TQ, Dang GH. Efficient degradation of methyl orange and methylene blue in aqueous solution using a novel Fenton-like catalyst of CuCo-ZIFs. Green Processing and Synthesis. 2022 Jan 1;11(1):71-83.

[7] Guo B, Ma J, Shi Y, Zheng K, Wu M, Ren G, Komarneni S. Co3O4/CoO ceramic catalyst: Bisulfite assisted catalytic degradation of methylene blue. Ceramics International. 2021 Oct 1;47(19):27617-23.

[8] Dong X, Lin Y, Ren G, Ma Y, Zhao L. Catalytic degradation of methylene blue by fenton-like oxidation of Ce-doped MOF. Colloids and Surfaces A: Physicochemical and Engineering Aspects. 2021 Jan 5;608:125578.

[9] Luo W, Chen Q, Ji L, Peng X, Huang G. Synergistic effect of various elements in Fe41Co7Cr15Mo14C15B6Y2 amorphous alloy hollow ball on catalytic degradation of methylene blue. Journal of Rare Earths. 2022 Apr 1;40(4):605-15.

[10] Lin S, Zhang T, Fu D, Zhou X. Utilization of magnesium resources in salt lake brine and catalytic degradation of dye wastewater by doping cobalt and nickel. Separation and Purification Technology. 2021 Sep 1;270:118808.

[11] Wolski L, Sobańska K, Walkowiak A, Akhmetova K, Gryboś J, Frankowski M, Ziolek M, Pietrzyk P. Enhanced adsorption and degradation of methylene blue over mixed niobium-cerium oxide–Unraveling the synergy between Nb and Ce in advanced oxidation processes. Journal of Hazardous Materials. 2021 Aug 5;415:125665.

[12] Zhang T, Ma Q, Zhou M, Li C, Sun J, Shi W, Ai S. Degradation of methylene blue by a heterogeneous Fenton reaction catalyzed by FeCo2O4-NC nanocomposites derived by ZIFs. Powder Technology. 2021 May 1;383:212-9.

[13] Kabel, K.I., Mady, A.H. and Rabie, A.M., 2021. Novel preparation of ferromanganese oxide based on hyperbranched polymer for peroxymonosulfate activation as a robust catalyst for the degradation of organic pollutants. Environmental Technology & Innovation, 22, p.101435.

[14] Zhang, S., Fan, Q., Gao, H., Huang, Y., Liu, X., Li, J., Xu, X. and Wang, X., 2016. Formation of Fe $_3O_4$@MnO_2 ball-in-ball hollow spheres as a high performance catalyst with enhanced catalytic performances. *Journal of Materials Chemistry A*, *4*(4), pp.1414-1422.

[15] Gao, M., Zhang, D., Li, W., Chang, J., Lin, Q., Xu, D. and Ma, H., 2016. Degradation of methylene blue in a heterogeneous Fenton reaction catalyzed by chitosan crosslinked ferrous complex. Journal of the Taiwan Institute of Chemical Engineers, 67, pp.355-361.

[16] Zhao Q, Zhang C, Tong X, Zou Y, Li Y, Wei F. Fe3O4-NPs/orange peel composite as magnetic heterogeneous Fenton-like catalyst towards high-efficiency degradation of methyl orange. Water Science and Technology. 2021 Jul 1;84(1):159-71.

[17] Yang L, Chen W, Sheng C, Wu H, Mao N, Zhang H. Fe/N-codoped carbocatalysts loaded on carbon cloth (CC) for activating peroxymonosulfate (PMS) to degrade methyl orange dyes. Applied Surface Science. 2021 May 30;549:149300.

[18] Gholami A, Mousavinia F. Eco-friendly approach for efficient catalytic degradation of organic dyes through peroxymonosulfate activated with pistachio shell-derived biochar and activated carbon. Environmental Technology. 2021 May 13:1-8.

[19] Gangwar A, Singh A, Pal S, Sinha I, Meena SS, Prasad NK. Magnetic nanocomposites of Fe3C or Ni-substituted (Fe3C/Fe3O4) with carbon for degradation of methylene orange and p-nitrophenol. Journal of Cleaner Production. 2021 Aug 1;309:127372.

[20] Das KC, Das B, Dhar SS. Effective catalytic degradation of organic dyes by nickel supported on hydroxyapatite-encapsulated cobalt ferrite (Ni/HAP/$CoFe_2O_4$) magnetic novel nanocomposite. Water, Air, & Soil Pollution. 2020 Feb;231(2):1-3.

[21] Sun X, Xu D, Dai P, Liu X, Tan F, Guo Q. Efficient degradation of methyl orange in water via both radical and non-radical pathways using Fe-Co bimetal-doped MCM-41 as peroxymonosulfate activator. Chemical Engineering Journal. 2020 Dec 15; 402:125881.

[22] Londoño-Calderón CL, Menchaca-Nal S, François NJ, Pampillo LG, Froimowicz P. Cupric Oxide Nanoleaves for the Oxidative Degradation of Methyl Orange without Heating or Light. ACS Applied Nano Materials. 2020 Feb 27;3(3):2987-96.

[23] Sun, B., Li, H., Li, X., Liu, X., Zhang, C., Xu, H. and Zhao, X.S., 2018. Degradation of organic dyes over fenton-like Cu_2O–Cu/C catalysts. *Industrial & Engineering Chemistry Research*, *57*(42), pp.14011-14021.

[24] Li Z, Wang F, Zhang Y, Lai Y, Fang Q, Duan Y. Activation of peroxymonosulfate by $CuFe_2O_4$-$CoFe_2O_4$ composite catalyst for efficient bisphenol a degradation: Synthesis, catalytic mechanism and products toxicity assessment. Chemical Engineering Journal. 2021 Nov 1; 423:130093.

[25] Kou, L., Wang, J., Zhao, L., Jiang, K. and Xu, X., 2021. Coupling of $KMnO_4$-assisted sludge dewatering and pyrolysis to prepare Mn, Fe-codoped biochar catalysts for peroxymonosulfate-induced elimination of phenolic pollutants. Chemical Engineering Journal, 411, p.128459.

[26] Ding Y, Li D, Zuo S, Guan Z, Ding S. Boron-doping accelerated Cu (II)/Cu (I) cycle for enhancing peroxymonosulfate activation. Separation and Purification Technology. 2022 Feb 1; 282:120086.

[27] Zuo S, Li D, Yang F, Xu H, Huang M, Guan Z, Xia D. Copper oxide/graphitic carbon nitride composite for bisphenol a degradation by boosted peroxymonosulfate activation: Mechanism of Cu-O covalency governs. Journal of Colloid and Interface Science. 2021 Dec 1; 603:85-93.

[28] Amiri MJ, Faraji A, Azizi M, Nejad BG, Arshadi M. Recycling bone waste and cobalt-wastewater into a highly stable and efficient activator of peroxymonosulfate for dye and HEPES degradation. Process Safety and Environmental Protection. 2021 Mar 1;147:626-41.

[29] Büker J, Angel S, Salamon S, Landers J, Falk T, Wende H, Wiggers H, Schulz C, Muhler M, Peng B. Structure-activity correlation in aerobic cyclohexene oxidation and peroxide decomposition over CoxFe3-xO4 spinel oxides. Catalysis Science & Technology. 2022.

[30] Wu Y, Su M, Xiao Y, Guang B, Liu Y. Heteropolyacid-Based Poly (ionic liquid) s for the Selective Oxidation of Cyclohexene to 2-Cyclohexene-1-one. Industrial & Engineering Chemistry Research. 2021 Dec 29.

[31] Pan H, Peng R, Zhu Z, Xu H, He M, Wu P. Highly Hydrophilic Ti− Beta Zeolite with Ti− Rich Exterior as Efficient Catalyst for Cyclohexene Epoxidation. Catalysts. 2022 Apr 12;12(4):434.

[32] Sudarsanam P, Singh N, Kalbande PN. Shape-controlled nanostructured MoO_3/CeO_2 catalysts for selective cyclohexene epoxidation. Catalysis Communications. 2022 Apr 1; 164:106433.

[33] Büker J, Huang X, Bitzer J, Kleist W, Muhler M, Peng B. Synthesis of Cu single atoms supported on mesoporous graphitic carbon nitride and their application in liquid-phase aerobic oxidation of cyclohexene. ACS catalysis. 2021 Jun 15;11(13):7863-75.

[34] Flores JG, Aguilar-Pliego J, Martin-Guaregua N, Ibarra IA, Sanchez-Sanchez M. Room-temperature prepared bimetallic nanocrystalline MOF-74 as catalysts in the aerobic oxidation of cyclohexene. Catalysis Today. 2021 Aug 28.

[35] Wu L, Han Y, Qi Y, Fu X, Chen R, Li J. Catalytic Oxidation of Cyclohexene by H_2O_2 Over Pd (II)-Complex Catalyst in a Heterogeneous System. Catalysis Letters. 2022 Jan 31:1-0.

[36] Santibáñez L, Escalona N, Torres J, Kremer C, Cancino P, Spodine E. CuII-and CoII-Based MOFs:{[La2Cu3 (μ-H_2O)(ODA) 6 (H2O) 3]· 3H2O} n and {[La2Co3 (ODA) 6 (H2O) 6]· 12H2O} n. The Relevance of Physicochemical Properties on the Catalytic Aerobic Oxidation of Cyclohexene. Catalysts. 2020 May;10(5):589.

[37] Mal DD, Kundu J, Pradhan D. CuO {001} as the Most Active Exposed Facet for Allylic Oxidation of Cyclohexene via a Greener Route. ChemCatChem. 2021 Jan 12;13(1):362-72.

[38] Jodłowski PJ, Kurowski G, Dymek K, Jędrzejczyk RJ, Jeleń P, Gancarczyk A, Węgrzynowicz A, Sawoszczuk T, Sitarz M. In situ deposition of M (M= Zn; Ni; Co)-MOF-74 over structured carriers for cyclohexene oxidation-Spectroscopic and microscopic characterisation. Microporous and Mesoporous Materials. 2020 Aug 15;303:110249.

[39] Duan M, Wang X, Peng W, Liu D, Cheng Q, Yang Q. Co (II) Schiff Base Complex Supported on Nano-Silica for the Aerobic Oxidation of Cyclohexene: Reaction Pathways and Overoxidation on the Experimental and Calculated Mechanism. ChemistrySelect. 2021 Mar 26;6(12):2869-77.

[40] Lu YJ, Janmanchi D, Natarajan T, Lin ZH, Wanna WH, Hsu IJ, Tzou DL, Ayalew Abay T, Yu SS. Silver Cyanide Powder-Catalyzed Selective Epoxidation of Cyclohexene and Styrene with its Surface Activation by H_2O_2 (aq) and Assisted by CH_3CN as a Non-Innocent Solvent. ChemCatChem.: e202200030.

[41] Awoke Y, Chebude Y, Díaz I. Ti-PMO materials as selective catalysts for the epoxidation of cyclohexene and vernonia oil. Catalysis Today. 2022 May 1;390:246-57.

[42] Qadir MI, Baptista DL, Dupont J. Effect of Support Nature on Ruthenium-Catalyzed Allylic Oxidation of Cycloalkenes. Catalysis Letters. 2022 Jan 6:1-8.

[43] Büker J, Alkan B, Fu Q, Xia W, Schulwitz J, Waffel D, Falk T, Schulz C, Wiggers H, Muhler M, Peng B. Selective cyclohexene oxidation with O_2, H_2O_2 and *tert*-butyl hydroperoxide over spray-flame synthesized LaCo 1− x Fe x O 3 nanoparticles. Catalysis Science & Technology. 2020;10(15):5196-206.

[44] Kurowski G, Jeleń P, Sitarz M, Jodłowski PJ. Spectroscopic and microscopic studies of Co, Ce, and Pd containing gamma-alumina as catalysts for cyclohexene oxidation. Journal of Molecular Structure. 2022 Aug 5; 1261:132880.

[45] L. Niu, G. Zhang, G. Xian, Z .Ren, T .Wei, Q. Li, Y. Zhang, Z. Zou. Tetracycline degradation by persulfate activated with magnetic γ-Fe_2O_3/CeO_2 catalyst: performance, activation mechanism and degradation pathway. Separation and Purification Technology. 259 (2021) 118156.

[46] Amasha M, Baalbaki A, Ghauch A. A comparative study of the common persulfate activation techniques for the complete degradation of an NSAID: the case of ketoprofen. Chemical Engineering Journal. 2018 Oct 15; 350:395-410.